Minerals Engineering 23 (2010) 691–697

Contents lists available at ScienceDirect

Minerals Engineering

journal homepage: www.elsevier.com/locate/mineng

A comparison of the electrochemical behaviors of pyrite and chalcopyrite in a NaCl solution at room temperature and under differential stress

Qingyou Liu, Heping Li *

Laboratory for Study of the Earth's Interior and Geofluids, Institute of Geochemistry, Chinese Academy of Sciences, Guiyang 550 002, China

ARTICLE INFO

Article history:
Received 18 January 2010
Accepted 28 April 2010

Keywords:
Pyrite
Chalcopyrite
Polarization curve
Electrical impedance spectroscopy
Differential stress

ABSTRACT

Electrochemical behaviors of pyrite and chalcopyrite were studied by measuring polarization curves and electrochemical impedance spectroscopy (EIS) in a NaCl solution at room temperature and under differential stress. The results from differential stress experiments show that there is a negative linear relation between potential difference and elastic stress. The corrosion current density distinctly increased, and the corrosion potential became more negative with an increase in differential stress. The charge transfer electrical resistance increased, the double layer capacitance decreased, and other characteristic parameters are observed with increasing differential stress. The experimental results are significant for sulfide mineral engineering. By using different equivalent electrical circuits, the point defect model, and corrosion theory, we explain the experimental results theoretically.

1. Introduction

Pyrite, one of the major minerals accumulating gold, and chalcopyrite, one of the most abundant copper sulfide minerals (and the major commercial source of copper), both possess the properties of a semi-conductor, and when oxygen and other oxidizing ions are present, electrochemical oxidation may occur. These electrochemical oxidations not only have an important effect on geochemical processes, such as ore geochemistry (Sun and Pfittmann, 1997; Lindsay et al., 2009) and environmental geochemistry (Moncur et al., 2005; Seal et al., 2008; Dinelli et al., 1998, 2001), but they also broadly affect the exploitation and use of sulfide minerals by human beings (Crozier, 1991; Tolley et al., 1996; Kocabağ and Güler, 2007). Not surprisingly, a vast amount of work has been published in the area of pyrite and chalcopyrite electrochemical behavior.

To better understand the electrochemical behavior of pyrite and chalcopyrite, the most vital thing is to understand their electrochemical interaction mechanisms. In most cases, pyrite is under acid solution and is oxidized by Fe^{3+} and dissolved oxygen. Holmes and Crundwell (2000) used the electrochemical technique of voltammetry to study the kinetics of the oxidation and reduction half-reaction of pyrite in a solution with presence of Fe^{3+} and dissolved oxygen. Using the electrochemical technique of potentiometry, they also studied the kinetics of the overall reaction. Their results indicate that the observations of half-order kinetics and the oxygen in the sulfate product arising from the water are both a direct consequence of the electrochemical mechanism. Kelsall et al. (1999) investigated the electrochemical oxidation of pyrite in aqueous electrolytes using electrochemical techniques, in situ Fourier transform infrared spectroscopy, ex situ X-ray photoelectron spectroscopy, and ion chromatography. The results show that the electrochemical oxidation of pyrite involves a complex set of reaction steps, in series and in parallel, ultimately producing Fe^{2+}/Fe^{3+} and $S/S_2O_3^{2-}/HSO_4^-$, depending on the pH and potential. The proposed mechanism for this process was discussed by using energy band and molecular orbital theories. Biegler and Swift (1979) used coulometry at a constant potential and analysis of products from pyrite oxidation in acid solution to study the same system. They conclude that the process involves a combination of the reactions $FeS_2 + 8H_2O \rightarrow Fe^{3+} + 2SO_4^{2-} + 16H^+ + 15e^-$ and $FeS_2 \rightarrow Fe^{3+} + 2S^0 + 3e^-$. Following this work, they postulated a mechanism for sulfate formation involving adsorbed oxygen-containing intermediates and the kinetics analyzed under Temkin adsorption conditions.

Similar to pyrite, most studies on chalcopyrite electrochemical behavior have been studied in acid solution (Holliday and Richmond, 1990; Gómez et al., 1996; Lu et al., 2000; Farquhar et al., 2003). Holliday and Richmond (1990) investigated the anodic dissolution of chalcopyrite ($CuFeS_2$) in acidic solutions using cyclic voltammetry with a rotating disc and ring-disc electrodes, as well as galvanostatic methods. They concluded that oxidation occurs by a sequential mechanism: there is an initial rate-determining step to produce the adsorbed copper(II) ion and then a reaction to produce the iron(II) ion. The final ratio of aqueous iron(II) to aqueous copper(II) was determined to be 5:1. Gómez et al. (1996) studied the electrochemical response of a massive chalcopyrite electrode

* Corresponding author.
E-mail address: liheping123@yahoo.com (H. Li).

0892-6875/$ - see front matter © 2010 Elsevier Ltd. All rights reserved.
doi:10.1016/j.mineng.2010.04.005

at two different temperatures, 25 °C and 68 °C, under an acidic medium. Their experimental results at both temperatures were similar and confirmed that, during the anodic dissolution of chalcopyrite, a passive film is formed on the surface that restricts the oxidation reactions in the medium by diffusion control of the film. The different responses at the temperatures tested are due to the differing physical structures of the complex films of the electrochemically formed sulfides, polysulfides, and elemental sulfur. Lu et al. (2000) used carbon paste electrodes to study the electrochemical oxidation of concentrated chalcopyrite in a mixed chloride–sulfate electrolyte. They pointed out that when chloride ions are present, the oxidation of the mineral significantly enhances both transient and steady-state techniques. Farquhar et al. (2003) studied the electrochemical oxidation of chalcopyrite at pH 4 using voltammetry, coulometry, X-ray photoelectron spectroscopy, and both ex situ and in situ atomic force microscopy. Their results indicate that, between 500 and 650 mV, there is an anodic oxidation peak prior to the onset of the main decomposition reactions. At 500 and 650 mV, the loss of Cu from the surface increases by a factor of 2 and 6, respectively. Oxidation at 500 mV is formats of a mixed oxide or hydroxide of iron, coincident with islands (<0.15 mm wide) of reaction products. The surface coverage of these islands increases with the amount of charge passed. Oxidation at 650 mV occurs by a similar process with a greater island surface coverage and a more deeply altered surface. Others have studied the electrochemical behavior of chalcopyrite in alkaline solutions (Velásquez et al., 1998), their experimental results shows two peaks in the positive sweep direction, which can be related to an oxidation process at the electrode surface that involves the formation of Fe_2O_3 and CuO, giving rise to an irregular surface layer of the electrode with islands of different chemical compositions. The X-ray photoelectron spectroscopy results confirm the formation of Fe_2O_3 and CuO at the electrode surface and their stability against decomposition at the reduction potential.

In summary, previous work concerning the electrochemical behaviors of pyrite and chalcopyrite mainly focused on conditions without stress. However, whether the sulfide minerals are being exploited by human beings or simply experiencing geochemical processes, stress is acting on them at all times. As a result, strain energy is transformed into electrochemical energy, changing their electrode potential, which must be considered a major influence on the electrochemical behaviors of these sulfide minerals. On the other hand, as one of the most common media used to leach sulfides (Winand, 1991) and study their solubility kinetics (Ohmoto et al., 1994), as well as one of the most common minerals composing the earth's crust (Bailey et al., 2002) and one of the most common components of mine waters (Bowell and Bruce, 1995; Silva et al., 2009), NaCl has an important effect on the electrochemical behaviors of pyrite and chalcopyrite. For the above reasons, the aim of this work was to study the electrochemical responses of massive pyrite and chalcopyrite in a NaCl solution under differential stresses to understand their dissolution kinetics and electrochemical mechanisms under stress action and, hence, to provide the experimental basis for sulfide mineral engineering.

2. Materials and methods

2.1. Preparation of the FeS_2/$CuFeS_2$ electrodes and reagents

We prepared FeS_2 and $CuFeS_2$ electrodes from dense, massive natural pyrite (origin, Yunfu mine, China) and chalcopyrite (origin, Daye mine, China) samples, respectively. They were cut and shaped into 10 mm × 10 mm × 40 mm blocks. Electron microprobe analysis confirmed that the pyrite sample Fe and S (wt.%) were 46.89 and 52.96%, respectively, and chalcopyrite Fe, Cu, and S (wt.%) were 30.70, 34.04, and 34.67%, respectively. Before the experiments, a fresh electrode surface was prepared by $1^{\#}$–$5^{\#}$ metallographic abrasive papers, cleaning with filter paper, and rinsing with acetone until clean. After each experiment, the used electrode was polished and reused.

The electrolyte was prepared from analytical grade chemicals and doubly distilled water containing 0.1 M NaCl. During all of the experiments, the electrochemical cell, which we made of rigid polytetrafluoroethylene, was filled with NaCl solution without purging the dissolved oxygen.

2.2. Instrumentation and methods

All of the mineral stress experiments were carried out on an electronic universal testing machine controlled by a computer. Two resistance strain gauges were stocked on the pyrite and chalcopyrite electrode surfaces, in the axial and lateral directions, respectively. Then, depending on the dynamic & static strain testing system, the axial stress, axial strain, and lateral strain data were all recorded. For comparison, rapid and continuously varying axial stresses (0, 2.0×10^5, 4.0×10^5, and 6.0×10^5 Pa) were imposed on the electrode during potential, polarization curve, and electrical impedance spectroscopy experiments, respectively.

The experiments were conducted using a stationary electrode in an air-conditioned room at 25 ± 1 °C.

3. Results and discussion

3.1. Stress–electrode potential experiments

An Agilent 34410A high-precision digital multimeter connected to a computer was used to measure the electrode potential. The pyrite (or chalcopyrite) electrode and saturated calomel electrode (SCE), through a Luggin capillary salt bridge composed of a standard two-electrode system, were partially placed in a rigid polytetrafluoroethylene cell (60 ml capacity) filled with NaCl solution. The exposed area of the mineral electrode in the electrolyte was 4 cm^2. All potentials recorded in this study were relative to the SCE. The experimental arrangement is shown schematically in Fig. 1.

The electrode potentials of pyrite and chalcopyrite in a 0.10 M NaCl solution under rapid, continuously varying differential stresses (Fig. 2c) are presented in Fig. 2a and b, respectively. Fig. 2 shows that the electrode potentials of pyrite and chalcopyrite are obviously distinct under similar differential stresses, but they have similar change relations. Combining stress and strain conditions in the experiment allowed us to derive a stress–strain-potential difference chart shown as Fig. 3. From this figure we can determine whether to pyrite or chalcopyrite, their axial stress and axial stain, along with the axial stress and lateral strain, all have a positive linear relation. These data indicate that the axial stresses acting on the pyrite (or chalcopyrite) electrode were elastic, and the electrode experienced an elastic strain. In addition, we also determined

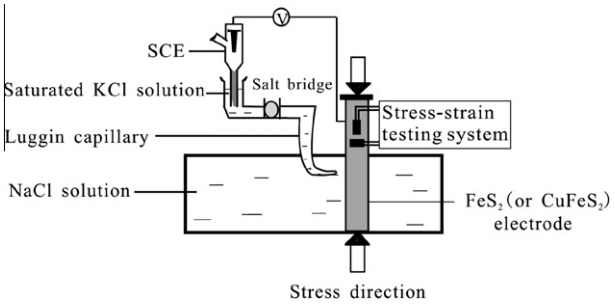

Fig. 1. Schematic diagram showing the stress-potential experimental arrangement.

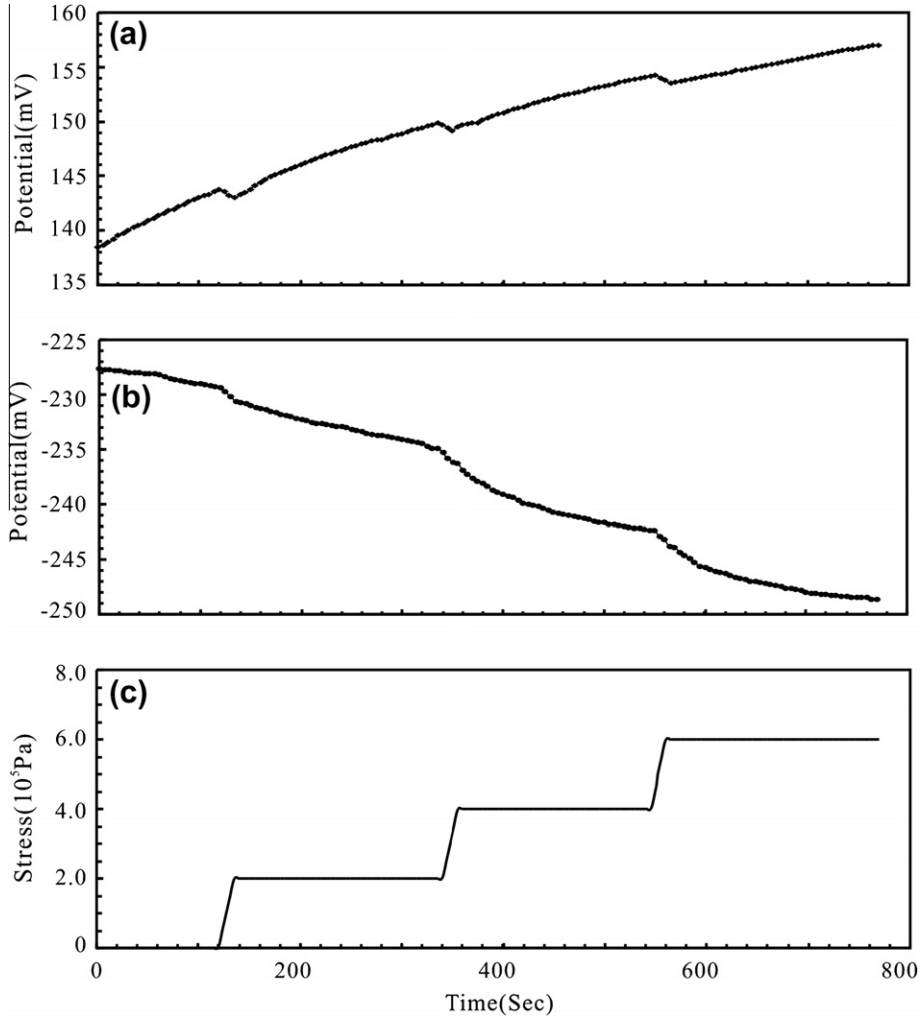

Fig. 2. Variations of the pyrite (a) and chalcopyrite (b) electrode potential in a 0.10 M NaCl solution under rapid, continuously varying axial stresses (c).

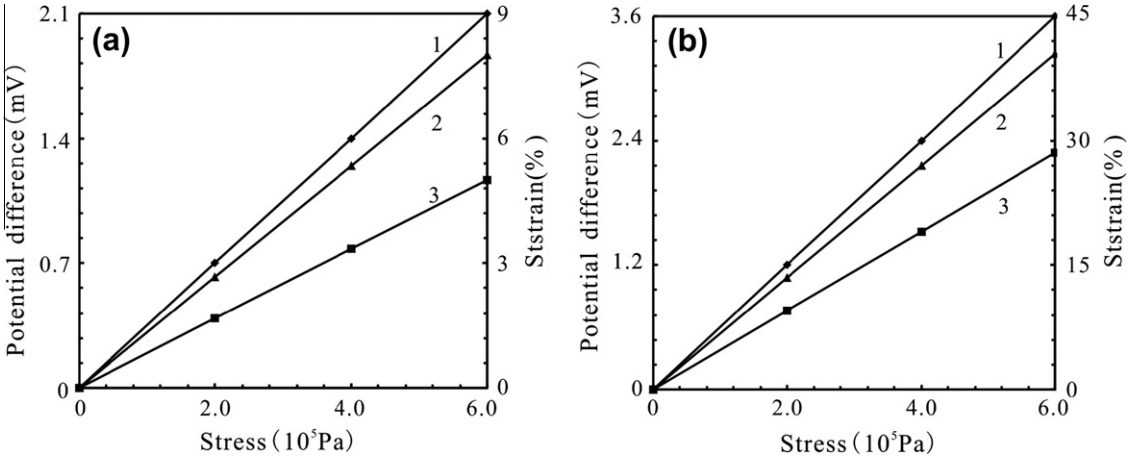

Fig. 3. Charts of the electrode potential difference-stress–strain for pyrite (a) and chalcopyrite (b). (1) Axial stress–electrode potential difference, (2) axial stress–axial strain, and (3) axial stress–lateral strain.

that the axial stress and the electrode potential had a negative linear relation.

If we define the sulfide mineral electrode potential as φ_H^{MS}, when the electrode is under elastic stress conditions, mechanical elements do not affect the electrolyte solution, and the chemical potential of reducible ions in solution does not change, although the chemical potential of the sulfide mineral electrode does. We can deduce that the electrode potential difference for stress is $\Delta\varphi_H^{MS} = -\frac{VdP}{ZF}$ (Liu et al., 2009), where V is the sulfide mineral molar volume, Z is the electron transfer number, and F is the Faraday

constant. The equation shows that there is a negative linear relation between the sulfide mineral electrode potential difference and the stress action, and it is only affected by its own character. The experimental results shown in Figs. 2 and 3 are consistent with this electrochemical theory.

3.2. Stress–polarization curve experiments

The polarization curve measurements were performed with a Parstat-2263 equipped with a PowerSuite system. The working electrode was the studied pyrite (or chalcopyrite) electrode with an exposed area of 4 cm^2, and the counter and reference electrodes were a platinum and SCE electrode, respectively. The potentials are reported with respect to the latter. The polarization scan was carried out from −250 mV vs. open circuit potential (E_{OC}) to + 250 mV vs. E_{OC}, at a rate of 1 mV/s. Data were recorded after a 30 min immersion in the working solution. Experimental controls and data analysis were carried out using PowerCorr software (Parstat Princeton Applied Research).

Pyrite and chalcopyrite Tafel plots are illustrated in Figs. 4 and 5, respectively. The two figures show that with increasing stress, the anode curve shape steepness, and the whole curve shifts toward more negative values along the vertical axis for pyrite and chalcopyrite. Comparing Figs. 4 and 5, the chalcopyrite electrode Tafel curves shifted to the right and moved toward more positive values on the vertical axes. Through Tafel extrapolation, the corrosion potential, corrosion current density, and Tafel slope were obtained; these data are listed in Table 1.

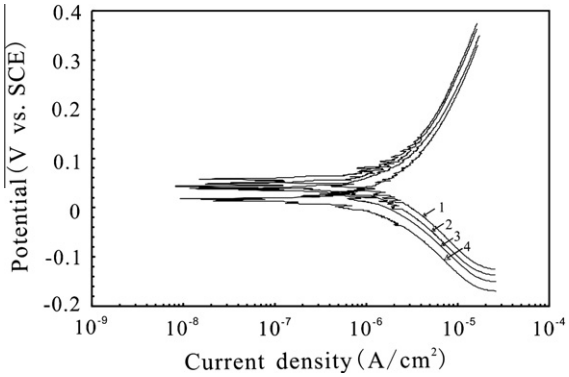

Fig. 5. Tafel plots for the chalcopyrite electrode in a 0.10 M NaCl solution under different axial stresses. (1) 0, (2) 2.0×10^5, (3) 4.0×10^5, and (4) 6.0×10^5 Pa.

As shown in Table 1, in the same concentration NaCl solution and with increasing stress, both the pyrite and chalcopyrite corrosion current densities increased, and the corrosion potential became more negative. At the same time, the anode Tafel slope varied more than the cathode's. Furthermore, under the same stress conditions, the chalcopyrite corrosion current density was obviously higher than that of pyrite, and the corrosion potential shifted toward more positive values. These results agree well with the previously reported (Rao and Finch, 1988) rest potentials of pyrite and chalcopyrite and were further corroborated with the following EIS study.

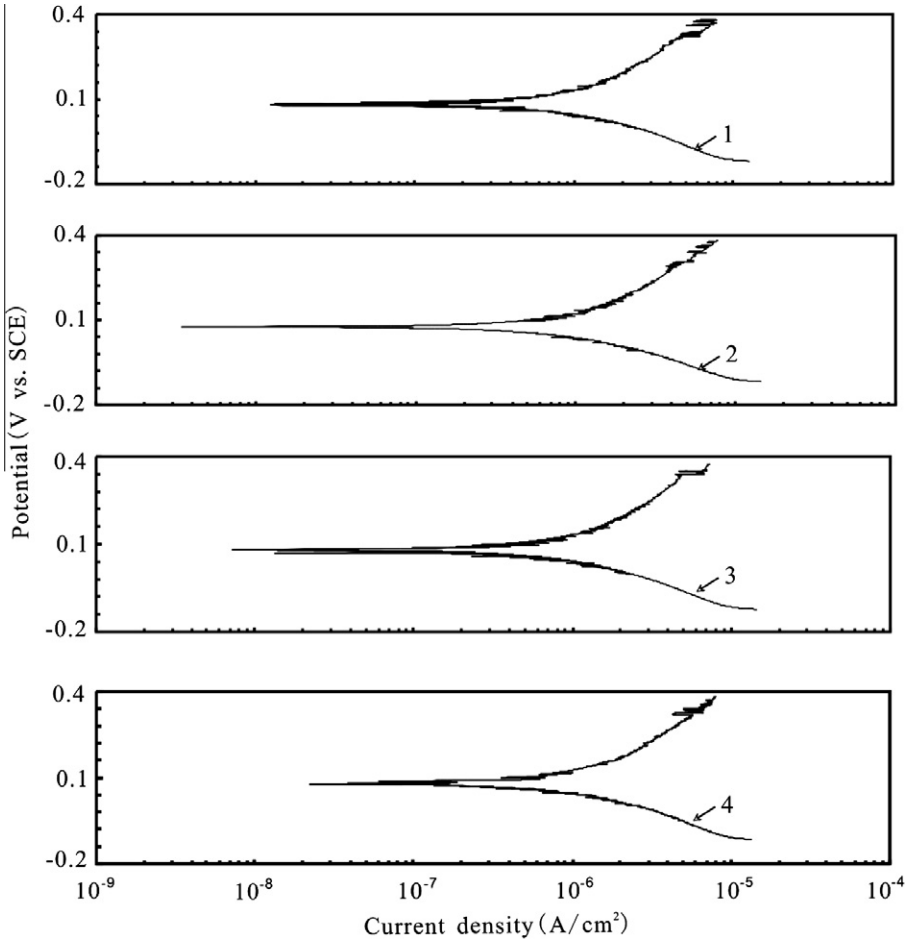

Fig. 4. Tafel plots for the pyrite electrode in a 0.10 M NaCl solution under different axial stresses. (1) 0, (2) 2.0×10^5, (3) 4.0×10^5, and (4) 6.0×10^5 Pa.

Table 1
Electrochemical corrosion parameters of the FeS_2/$CuFeS_2$ samples from Tafel tests in 0.10 M NaCl solution under different stresses.

Electrode	Stress (10^5 Pa)	E_{corr} (mV)	i_{corr} (μA cm^{-2})	β_c (mV)	β_a (mV)
FeS_2	0	85.402	3.272	210.701	349.295
	2	84.040	4.636	215.436	360.198
	4	82.922	5.194	224.979	405.325
	6	80.368	6.169	231.332	420.345
$CuFeS_2$	0	−16.037	9.214	159.104	387.280
	2	−17.610	9.640	163.658	417.913
	4	−17.819	9.985	166.298	426.075
	6	−20.030	10.90	169.339	436.222

E_{corr}: corrosion potential; i_{corr}: corrosion current density; β_c: cathode Tafel slope; β_a: anode Tafel slope.

3.3. Stress–electrical impedance spectroscopy (EIS) experiments

EIS measurements are often used to obtain information about the properties of a system, such as the presence of defects, reactivity of the interface, adhesion, and barrier properties. Knowledge of these parameters is very useful for predicting corrosive behavior (Bonora et al., 1996). In this work, we used EIS experiments to study the micro-kinetics parameters of the covering layer and double layer (e.g., charge transfer and double layer capacitance) of the pyrite and chalcopyrite electrode in contact with a naturally aerated 0.10 M NaCl solution under rapid and continuously varying elastic axial stresses (0, 2.0×10^5, 4.0×10^5, and 6.0×10^5 Pa). All of the EIS measurements were carried out at an open circuit potential in the 1×10^5 to 0.01 Hz frequency range, using a Parstat-2263 interfaced with a PC. The amplitude of the sinusoidal voltage was 5 mV rms. Data were recorded after 1 h of immersion in the working solution. The equivalent circuit model fitting for the AC impedance was evaluated using ZSimpWin (Version 3.10) software from PAR.

Fig. 6a presents the bode plots for the pyrite electrode in a 0.10 M NaCl solution under different elastic axial stresses, where two time constants can be clearly observed by the two obviously distorted capacitive loops. The Nyquist diagram (Fig. 6b) also reflects this character. The EIS spectra fitted well with the Randles equivalent electrical circuit (Fig. 6c), where R_s is the solution resistance, R_t is the charge transfer resistance, a constant phase element (CPE) substituted for the double layer capacitance connection of the Helmholtz layer and the surface film, and W is the Warburg diffusion resistance. The values of these parameters are given in Table 2. From this table, we can see that with the stress increasing from 0 to 6.0×10^5 Pa, the charge transfer resistance R_t decreased from 4523 to 3806 Ω cm^2, the CPE capacitance parameter Y_0 increased from 7.459E-7 to 8.195E-7 S cm^{-2} s^{-n}, the exponent n decreased from 0.7770 to 0.7696, and the Warburg diffusion resistance Y_0 increased from 0.0008479 to 0.001600 S cm^{-2} s$^{-0.5}$.

The impedance spectra for chalcopyrite obtained in a 0.10 M NaCl solution under different elastic axial stresses are presented as Bode plots in Fig. 7a, as a Nyquist diagram in Fig. 7b, and may be described by a simple equivalent circuit model, as shown in Fig. 7c. The equivalent circuit model contains a solution resistance (R_s) in series with the parallel network of the charge transfer resistance (R_t) and a constant phase element (CPE) substituted for the double layer capacitance. The impedance is shown as: $Z_{CPE} = [Y_0(j\omega)^n]^{-1}$ (Cole and Cole, 1941), where Y_0 is the capacitance parameter, j is the imaginary constant, and n is the parameter that characterizes the deviation of the system from ideal capacitive ($n = 1$). The parameters R_s, Y_0, n, and R_t are shown in Table 2. The impedance parameters listed in Table 2 suggest that stress had an important effect on the behavior of the chalcopyrite electrode. With the stress increasing from 0 to 6.0×10^5 Pa, the charge transfer resistance R_t decreased from 3120 to 2523 Ω cm^2, the CPE capacitance parameter Y_0 increased from 0.001532 to 0.001611 S cm^{-2} s^{-n}, and the exponent n decreased from 0.6165 to 0.5626.

According to the above stress-EIS experiments, with increasing stress, the charge transfer resistance R_t and exponent n both decrease, whereas the CPE capacitance parameter Y_0 and Warburg diffusion resistance Y_0 both increase for pyrite and chalcopyrite. It is well known that the charge transfer resistance represents the electrode polarization resistance, and its value characterizes the ease of electron transfer on the electrode surface. Further, the capacitance parameter Y_0 represents the electric double layer at the mineral–water interface and characterizes the ease of ion diffusion between the electric double layers. Thus, it is simple to understand that when the elastic axial stresses increase, the pyrite or chalcopyrite electrode gains more strain energy, which changes into electrochemical energy such that the electron transfer on the electrode surface is easier (i.e., the charge transfer resistance R_t decreases). Similarly, with increasing stress, the double layer that connects the Helmholtz layer and the surface film, whose "distance" decreases, must induce an increase in the CPE capacitance parameter Y_0, and ion diffusion becomes easier (i.e., the W capacitance parameter Y_0 increases).

Comparing the pyrite and chalcopyrite stress-EIS experiments, we found that for the same experimental conditions, chalcopyrite had a smaller transfer resistance R_t and exponent n and a larger electric double layer capacitance parameter Y_0. All of these param-

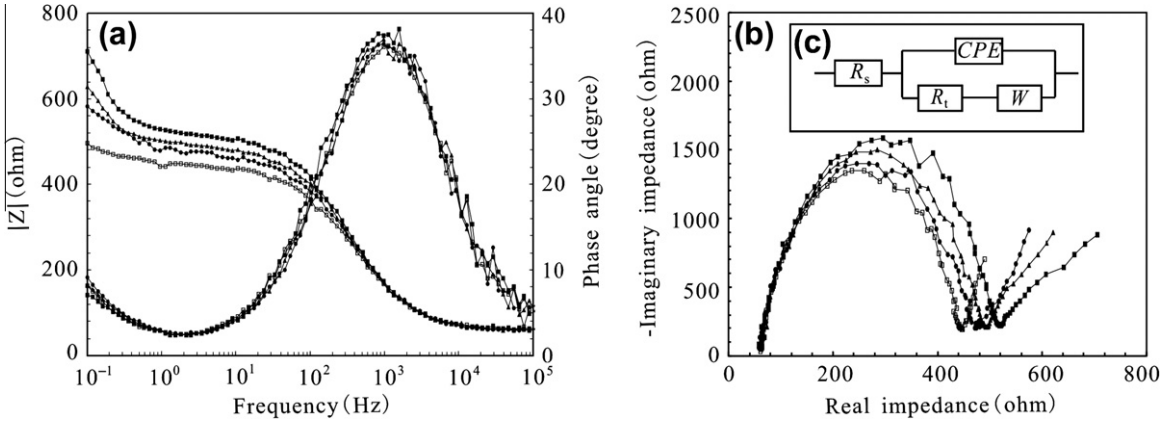

Fig. 6. Bode plots and phase angles (a), Nyquist impedance spectra (b), and equivalent circuit (c) for pyrite under different axial stresses in 0.10 M NaCl solutions. (■) 0, (▲) 2.0×10^5, (●) 4.0×10^5, and (□) 6.0×10^5 Pa.

Table 2
Impedance parameters of the FeS_2/$CuFeS_2$ samples in 0.10 M NaCl solution under different stresses.

Electrode	Stress (10^5 Pa)	R_s (Ω cm^2)	CPE, Y_0 (S cm^{-2} s^{-n})	n	R_t (Ω cm^2)	W, Y_0 (S cm^{-2} s$^{-0.5}$)
FeS_2	0	602.9	7.459E-7	0.7770	4523	0.0008479
	2	596.8	7.473E-7	0.7762	4239	0.0009934
	4	574.0	7.852E-7	0.7700	4087	0.001020
	6	575.3	8.195E-7	0.7696	3806	0.001600
$CuFeS_2$	0	1314	0.001532	0.6165	3102	–
	2	1352	0.001580	0.6142	2730	–
	4	1277	0.001593	0.5861	2692	–
	6	1355	0.001611	0.5626	2523	–

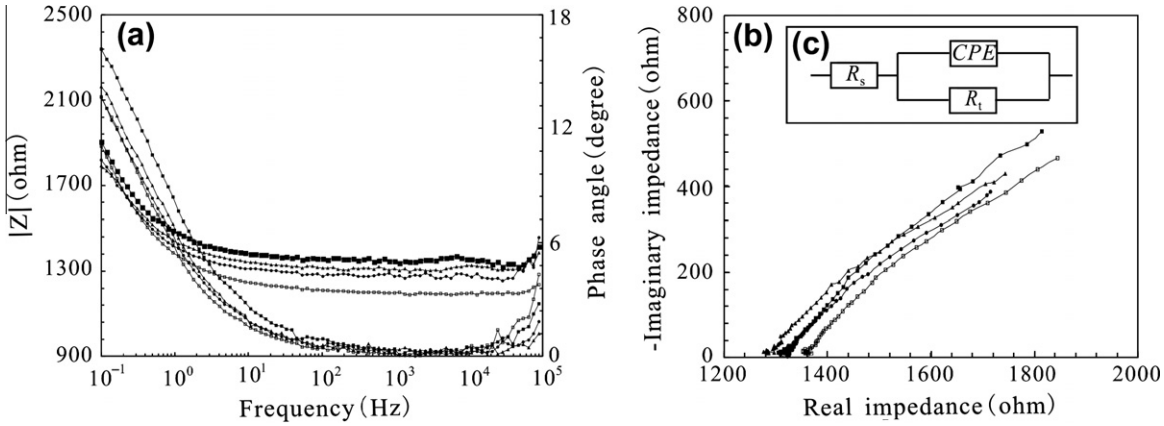

Fig. 7. Bode plots and phase angles (a), Nyquist impedance spectra (b), and equivalent circuit (c) for chalcopyrite under different axial stresses in 0.10 M NaCl solutions. (■) 0, (▲) 2.0×10^5, (●) 4.0×10^5, and (□) 6.0×10^5 Pa.

eter characters agree with the natural characteristics of pyrite and chalcopyrite, i.e., that chalcopyrite has a more negative rest potential and is easier to oxidize. The stress-EIS experimental results also agree well with the stress-polarization curve experimental results.

When the pyrite or chalcopyrite electrodes are immersed in the NaCl electrolyte, anode and oxidation reactions occur on their surfaces (Holmes and Crundwell, 2000):

$$\text{Anode}: FeS_2 \rightarrow Fe^{2+} + 2S^0 + 2e^- \quad (1)$$

$$CuFeS_2 \rightarrow Cu^{2+} + Fe^{2+} + 2S^0 + 4e^- \quad (2)$$

whereas the Pt electrode acts as a cathode, and the dissolved oxygen reduction reaction occurs on its surface:

$$\text{Cathode}: O_2 + H_2O + 4e^- \rightarrow 4OH^- \quad (3)$$

According to rest potential theory, for pyrite, which has a "high" positive rest potential compared to chalcopyrite, electrode reaction (1) must be easier than reaction (2), so inducing the S^0 film coverage conditions on the electrode surfaces is different. In other words, pitting corrosion occurs easily on the chalcopyrite electrode surface. Thus, there are two time constants in the pyrite stress experiments and only one time constant in the chalcopyrite stress experiments. Here, we propose that for the pyrite stress experiments, the first time constant in the high frequency region is a fast charge transfer process between pyrite and O_2, and the second in the low frequency region results from the diffusion of anion vacancies generated at the pyrite-film interface across the growing S^0 film and their consumption at the film-solution interface.

4. Implications

From the above experiments, we found that differential stress markedly affected the electrode potential of sulfide minerals, and consequently affected their electrochemical behavior. Such stresses must ultimately affect their geochemical processes and the exploitation and use of sulfide minerals by human beings.

Much of the earth's crust is subject to stress. Khilyuk and Chilingar (2000) indicate that excessive accumulation of stresses is the primary cause of all seismic events. Thus, continuous surveillance of strains and tilts to detect anomalous changes in the systematic records of strains and crustal movement may uncover the patterns that precede earthquakes. However, when stress–strain measures are in severely to unmeasurable, continuous surveillance of electric field results using the sulfide mineral potential may be a good substitute method. On the other hand, differential stress affects the pressure solution mechanism of sulfide minerals and may well explain geochemistry phenomena, such as element activation, migration, concentration, and position in the shallow crust.

In the field of mineral engineering, the rest potential is acknowledged as the most crucial factor that affects mineral processing progress. For a single sulfide mineral, a change in stress conditions can activate the rest potential, resulting in increased metallurgical efficiency. However, when two sulfide minerals have similar rest potentials, the metallurgical efficiencies are usually very low. From the stress experiments, we found that various different electrode potentials gave the same stress, indicating that adding stress can increase the difference in their rest potential and thereby increase the overall metallurgical efficiency.

5. Conclusions

We studied the electrochemical behaviors of pyrite (FeS_2) and chalcopyrite ($CuFeS_2$) in 0.1 M NaCl solution under differential stresses using polarization curves and electrical impedance spectroscopy. Several conclusions can be drawn from this research:

(1) There was a negative linear relationship between the pyrite/chalcopyrite potential difference and the stress action, and it was only affected by their own character. The mathematical expression is: $\Delta\varphi_H^{MS} = -\frac{VdP}{ZF}$.
(2) Polarization curve experiments indicated that without changes to other conditions, increased differential stress leads to a higher corrosion current density and more negative corrosion potential. For the same experimental conditions, chalcopyrite has greater corrosion current density and more positive corrosion potential. These results show that stress can speed up the corrosion electrochemical behavior of pyrite and chalcopyrite; under the same conditions, chalcopyrite is more corrodible than pyrite; and
(3) Electrical impedance spectroscopy experiments indicated that without changes to other conditions, increasing the differential stress decreases the charge transfer resistance R_t and the exponent n, whereas the capacitance parameter Y_0 and the Warburg diffusion capacitance Y_0 increased. The results indicated the reason why increasing stress induces increased pyrite and chalcopyrite corrosion.

Acknowledgments

This work was financially supported by the National Natural Science Foundation of China (40803017; 40573046), the Large-scale Scientific Apparatus Development Program of Chinese Academy of Sciences (YZ200720), the Municipal Science and Technology Foundation of Guizhou Province, China (No. 2008GZ02240), and the West Light Foundation Doctor Cultivate Progress Foundation of the Chinese Academy of Sciences.

References

Bailey, R.A., Clark, H.M., Ferris, J.P., Krause, S., Strong, R.L., 2002. The Earth's Crust Chemistry of the Environment, second ed. pp. 443–482.
Biegler, T., Swift, D.A., 1979. Anodic behaviour of pyrite in acid solutions. Electrochem. Acta 24, 415–420.
Bonora, P.L., Deflorian, F., Fedrizzi, L., 1996. Electrochemical impedance spectroscopy as a tool for investigating underpaint corrosion. Electrochem. Acta 41, 1073–1082.
Bowell, R.J., Bruce, I., 1995. Geochemistry of iron ocher's and mine waters from Levant Mine. Cornwall. Appl. Geochem. 10, 237–250.
Cole, K.S., Cole, R.H., 1941. Dispersion and absorption in dielectrics. I. Alternating current characteristics. J. Chem. Phys. 9, 341–351.
Crozier, D.R., 1991. Sulphide collector mineral bonding and the mechanism of flotation. Miner. Eng. 4, 839–858.
Dinelli, E., Morandi, N., Tateo, F., 1998. Fine-grained weathering products in a waste disposal from the sulphide mines of the northern Apennines, Italy. Clay Miner. 30, 423–433.
Dinelli, E., Lucchini, F., Fabbri, M., Cortecci, G., 2001. Metal distribution and environmental problems related to sulfide oxidation in the Libiola copper mine area (Ligurian Apennines, Italy). J. Geochem. Explor. 74, 141–152.
Farquhar, M.L., Wincott, P.L., Wogelius, R.A., Vaughan, D.J., 2003. Electrochemical oxidation of the chalcopyrite surface. an XPS and AFM study in solution at pH 4. Appl. Surf. Sci. 218, 34–43.
Gómez, C., Figueroa, M., Muñoz, J., Blázquez, M.L., Ballester, A., 1996. Electrochemistry of chalcopyrite. Hydrometallurgy 43, 331–344.
Holliday, R.I., Richmond, W.R., 1990. An electrochemical study of the oxidation of chalcopyrite in acidic solution. J. Electroanal. Chem. 288, 83–98.
Holmes, P.R., Crundwell, F.K., 2000. The kinetics of the oxidation of chalcopyrite by ferric ions and dissolved oxygen: an electrochemical study. Geochem. Cosmochem. Acta 64, 263–274.
Kelsall, G.H., Yin, Q., Vaughan, D.J., England, K.E.R., Brandon, N.P., 1999. Electrochemical oxidation of pyrite (FeS_2) in aqueous electrolytes. J. Electroanal. Chem. 471, 116–125.
Khilyuk, L.F., Chilingar, G.V., Robertson Jr., John O., Endres, Bernard, 2000. Messages from the Earth's Crust. Gas Migr., 163–187.
Kocabağ, D., Güler, T., 2007. Two-liquid flotation of sulphides: an electrochemical approach. Miner. Eng. 20, 1246–1254.
Lindsay, M.B.J., Condon, P.D., Jambor, J.L., Lear, K.G., Blowes, D.W., Ptacek, C.J., 2009. Mineralogical, geochemical, and microbial investigation of a sulfide-rich tailings deposit characterized by neutral drainage. Appl. Geochem. 24, 2212–2221.
Liu, Q.Y., Li, H.P., Zhou, L., 2009. Experimental study of chalcopyrite–galena galvanic in a flowing system and its applied implications. Hydrometallurgy 96, 132–139.
Lu, Z.Y., Jeffrey, M.I., Lawson, F., 2000. An electrochemical study of the effect of chloride ions on the dissolution of chalcopyrite in acidic solutions. Hydrometallurgy 56, 145–155.
Moncur, M.C., Ptacek, C.J., Blowes, D.W., Jambor, J.L., 2005. Release, transport and attenuation of metals from an old tailings impoundment. Appl. Geochem. 20, 639–659.
Ohmoto, H., Hayashi, K., Kajisa, Y., 1994. Experimental study of the solubilities of pyrite in NaCl-bearing aqueous solutions at 250–350 °C. Geochem. Cosmochem. Acta 58, 2169–2185.
Rao, S.R., Finch, J.A., 1988. Galvanic interaction studies on sulphide minerals. Can. Metall. Q. 27, 253–259.
Seal II, R.R., Hammarstrom, J.M., Johnson, A.N., Piatak, N.M., Wandless, G.A., 2008. Environmental geochemistry of a Kuroko-type massive sulfide deposit at the abandoned Valzinco mine, Virginia, USA. Appl. Geochem. 23, 320–342.
Silva, E.F.d., Bobos, I., Matos, J.X., Patinha, C., Reis, A.P., Fonseca, E.C., 2009. Mineralogy and geochemistry of trace metals and REE in volcanic massive sulfide host rocks, stream sediments, stream waters and acid mine drainage from the Lousal mine area (Iberian Pyrite Belt, Portugal). Appl. Geochem. 24, 383–401.
Sun, Y.Z., Pfittmann, W., 1997. Metal accumulation during and after deposition of the Kupferschiefer from the Sangerhausen basin, Germany. Appl. Geochem. 12, 577–592.
Tolley, W., Kotlyar, D., Wagoner, V.R., 1996. Fundamental electrochemical studies of sulfide mineral flotation. Miner. Eng. 9, 603–637.
Velásquez, P., Gómez, H., Ramos-Barrado, J.R., Leinen, D., 1998. Voltammetry and XPS analysis of a chalcopyrite $CuFeS_2$ electrode. Colloids Surf. A: Physicochem. Eng. Aspects 140, 369–375.
Winand, R., 1991. Chloride hydrometallurgy. Hydrometallurgy 27, 285–316.